npj | Quantum Materials

www.nature.com/npjquantmats

ARTICLE OPEN

Two-gap superconductivity in $CaFe_{0.88}Co_{0.12}AsF$ revealed by temperature dependence of the lower critical field $H_{c1}^{c}(T)$

Teng Wang[1,2,3], Yonghui Ma[1,2,4], Wei Li[5,6], Jianan Chu[1,2,4], Lingling Wang[1], Jiaxin Feng[1,2,4], Hong Xiao[7], Zhuojun Li[1,2], Tao Hu[1,2], Xiaosong Liu[1,2,3] and Gang Mu[1,2]

Gap symmetry and structure are crucial issues in understanding the superconducting mechanism of unconventional superconductors. Here, we report an in-depth investigation on the out-of-plane lower critical field H_{c1}^{c} of fluorine-based 1111 system superconductor $CaFe_{0.88}Co_{0.12}AsF$ with $T_c = 21$ K. A pronounced two-gap feature is revealed by the kink in the temperature-dependent $H_{c1}^{c}(T)$ curve. The magnitudes of the two gaps are determined to be $\Delta_1 = 0.86$ meV and $\Delta_2 = 4.48$ meV, which account for 74% and 26% of the total superfluid density, respectively. Our results suggest that the local antiferromagnetic exchange pairing picture is favored compared to the Fermi surface nesting scenario.

npj Quantum Materials (2019)4:33 ; https://doi.org/10.1038/s41535-019-0173-0

INTRODUCTION

Superconducting (SC) mechanism is the central issue in the study of unconventional superconductors. Since the discovery of Fe-based superconductors (FeSCs),[1] many efforts have been made on this problem.[2] At the early stage, itinerant mechanism based on the weak correlation was accepted widely and the Fermi surface (FS) nesting (abbreviate as nesting scenario) was believed to be very crucial for the superconductivity.[3,4] Later on, this scenario was challenged by other studies,[5–8] especially by the discovery of $K_xFe_{2-y}Se_2$ system without hole type FS near the Γ point.[9–12] Consequently, the local antiferromagnetic exchange pairing scenario (abbreviate as local scenario), considering a stronger electron correlation, attracts more and more attentions.[13–16] Despite the distinct mechanisms mentioned above, the prospective physical manifestations may be rather subtle. For example, both of them predicted a sign-changed s-wave (S±) gap symmetry. However, the FSs with a better nesting condition tend to have a stronger pairing amplitude and larger SC gap in the itinerant mechanism,[17–19] while according to the local scenario, a larger SC gap should open on the smaller FS.[13] Typically, approximations were made in the theoretical models and a precise comparison to the experimental results is difficult. In the case of 122 system $Ba_{0.6}K_{0.4}Fe_2As_2$, for example, the larger SC gap was found to open on the FSs with a smaller size and a better nesting condition,[19–21] which could not discriminate these two theoretical proposals. Therefore, currently more delicate experiments are required.

Recently, clear progresses were made on the single-crystal growth of the fluorine-based 1111 system of FeSCs, i.e. CaFeAsF[22] and the Co-doped counterparts,[23] and systematic investigations have been carried out on this system.[24–31] Especially, it was found that the smaller FS around the Γ point (see the *α* FS in Fig. 4a) is much smaller than other FSs around *M* point and consequently shows a worse nesting condition,[27,32] as compared with the other larger FSs, which should benefit the identification of the above-mentioned itinerant and local mechanisms.

In this paper, we present a detailed investigation on the temperature dependence of the out-of-plane lower critical field $H_{c1}^{c}(T)$ of the high-quality $CaFe_{0.88}Co_{0.12}AsF$ single crystals. The lower critical field reflects the information of penetration depth and superfluid density, which is a good pointcut to investigate the intrinsic SC properties of FeSCs.[33–35] The data is described by a two-component-superfluid model with two SC gaps, $\Delta_1 = 0.86$ meV and $\Delta_2 = 4.48$ meV. Considering the weighting factors for the two components, we conclude that the larger gap is most likely opened on the smaller FS, which has a bad nesting condition with other FSs. Thus our results provide a clear identification and the local antiferromagnetic exchange pairing scenario is favored.

RESULTS

The dc magnetic susceptibility χ for the $CaFe_{0.88}Co_{0.12}AsF$ sample was measured under a magnetic field of 10 Oe in zero-field-cooling and field-cooling modes, which is presented in Fig. 1a. The $\chi - T$ curve shows a sharp SC transition, which reflects the homogeneity and high quality of our sample. The onset transition temperature T_c is about 21 K. The absolute value of magnetic susceptibility χ is over 95% after the demagnetization was considered, indicating a high SC volume fraction. The isothermal $M - H$ curves for the same sample are shown in Fig. 1b, c. The full magnetization curve shown in Fig. 1b is rather symmetric, illustrating a very low surface barrier for the flux lines when entering the sample. For the data in the low-field region as shown in Fig. 1c, one can see the evolution from the low-field linear

[1]State Key Laboratory of Functional Materials for Informatics, Shanghai Institute of Microsystem and Information Technology, Chinese Academy of Sciences, Shanghai 200050, China; [2]Center for Excellence in Superconducting Electronics (CENSE), Chinese Academy of Sciences, Shanghai 200050, China; [3]School of Physical Science and Technology, ShanghaiTech University, Shanghai 201210, China; [4]University of Chinese Academy of Sciences, Beijing 100049, China; [5]State Key Laboratory of Surface Physics and Department of Physics, Fudan University, Shanghai 200433, China; [6]Collaborative Innovation Center of Advanced Microstructures, Nanjing 210093, China and [7]Center for High Pressure Science and Technology Advanced Research, Beijing 100094, China
Correspondence: Gang Mu (mugang@mail.sim.ac.cn)

Received: 23 February 2019 Accepted: 6 June 2019
Published online: 02 July 2019

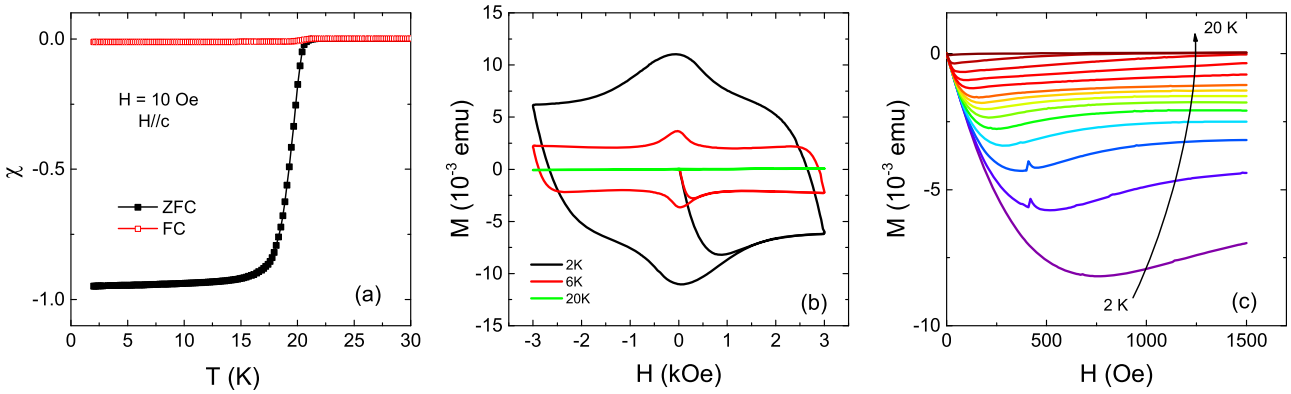

Fig. 1 Magnetization of the $CaFe_{0.88}Co_{0.12}AsF$ single crystal. **a** Temperature dependence of volume susceptibility measured in zero-field-cooled (ZFC) and field-cooled (FC) modes. **b** The full magnetization curves at three typical temperatures. **c** Field dependence of magnetic moment in the field region below 1500 Oe at different temperatures from 2 to 20 K. The intervals are 1 K/step in the range 2–10 K and 2 K/step in the range 10–20 K

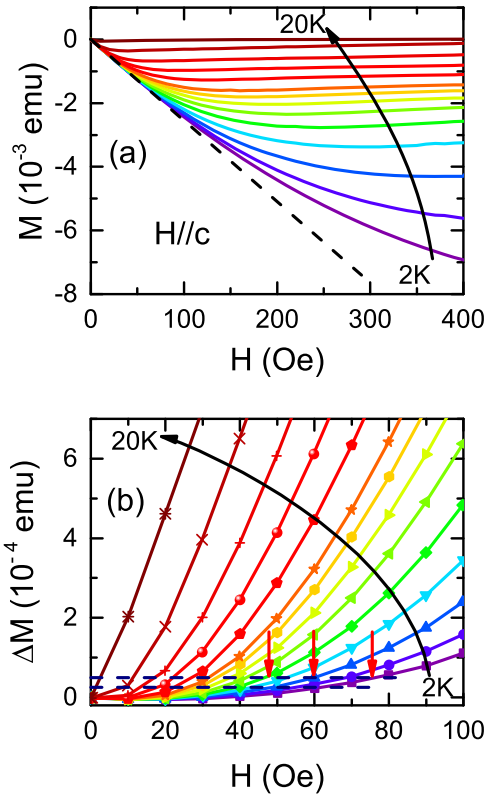

Fig. 2 Magnetization data in the low-field region. **a** Isothermal $M-H$ curves in the field range of 0–400 Oe. The black dashed line shows the linear fit in the low-field region, which is called Meissner line. **b** Deviation of magnetization data from the Meissner line. The two dashed lines are two different criteria for determining H_{c1}^c. Three red arrows indicate the positions of H_{c1}^c at 2, 4, and 6 K with criteria 1. The temperature intervals for **a** and **b** are the same as those in Fig. 1c

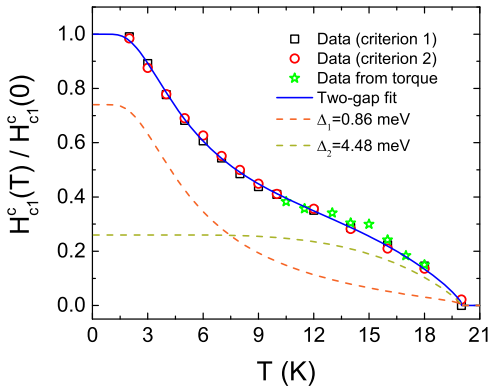

Fig. 3 The extracted $H_{c1}^c(T)$ (normalized by the zero-temperature value $H_{c1}^c(0)$) as a function of temperature. The data from two criteria are displayed in company with that from the magnetic torque measurements.[26] The solid line is the fitting curve using the two-gap model. The contributions of the two components with different gap magnitudes are also shown by the dashed lines

tendency to the crooked behavior with the increase of field. The former represents an ideal Meissner state and the latter reflects the penetration of field into the interior of the sample.

In order to have a clear impression for the data in low-field region, we show the enlarged view of the isothermal $M-H$ curves in Fig. 2a. The black dashed line represents the linear $M-H$ relation in the very low-field region, which is a consequence of the Meissner effect. Customarily this dashed line is called the Meissner line. We checked the deviation of the magnetization data from the Meissner line to have a solid determination for the onset point of the field penetration, i.e., H_{c1}^c. Field dependence of such a deviation ΔM is displayed in Fig. 2b. Two criteria, $\Delta M = 5\times10^{-5}$ emu and 2.5×10^{-5} emu equivalent to 2 Oe and 1 Oe respectively, are adopted for the determination of H_{c1}^c. As revealed by the two dashed lines in Fig. 2b, obviously the variation of criterion will affect the obtained H_{c1}^c values. Nevertheless, as shown in Fig. 3, the evolution behavior with temperature is not affected by the criterion. In addition, we found that the temperature dependent tendency from our measurements is also consistent with that obtained by the magnetic torque experiments,[26] as displayed by the green asterisks. So we will focus on the analysis of the normalized values $H_{c1}^c(T)/H_{c1}^c(0)$, which are more solid and reliable.

It is known that typically the FeSCs are in the local limit,[33] thus the local London model can be used. According to the local London model, the normalized superfluid density within the *ab* plane $\tilde{\rho}_s^{ab}$ has a close relation with the out-of-plane lower critical field H_{c1}^c:[33,34]

$$\tilde{\rho}_s^{ab}(T) = \frac{\lambda_{ab}^2(0)}{\lambda_{ab}^2(T)} = \frac{H_{c1}^c(T)}{H_{c1}^c(0)}. \quad (1)$$

Here, λ_{ab} is the penetration depth within the *ab* plane. Moreover, the FSs in the present system are nearly ideal cylinders[27,32] and the in-plane Fermi velocity is rather isotropic within the k_x-k_y

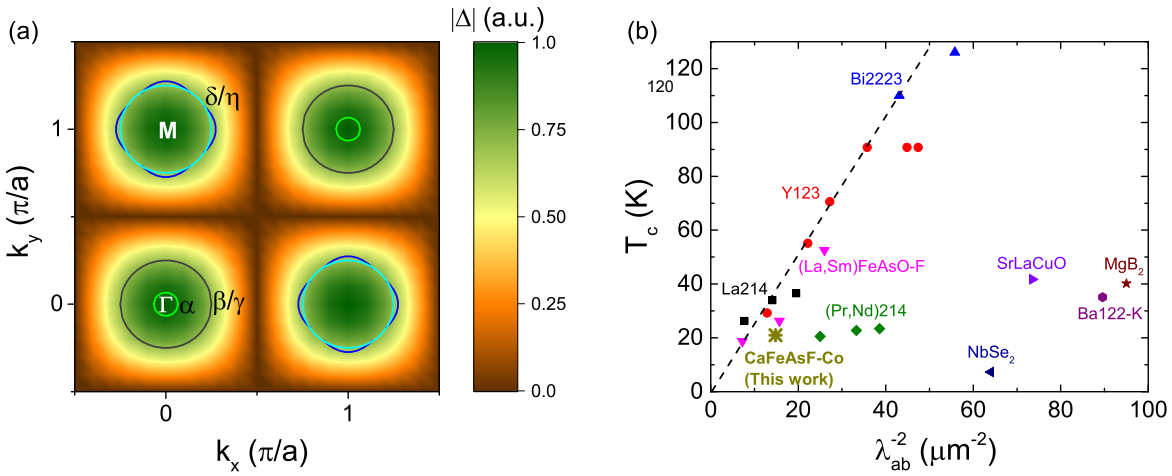

Fig. 4 Distribution of gap value and the Uemura Plot. **a** Theoretical SC gap value $|\Delta(k)| = \Delta_0|\cos k_x \cos k_y|$ as a function of the two-dimensional wave vector. The schematic five Fermi surfaces are also shown. **b** The correlations between T_c and λ_{ab}^{-2}, which is proportional to the superfluid density. Points for the cuprates (including $La_{2-x}Sr_xCuO_{4+\delta}$ (La214), $YBa_2Cu_3O_{7+\delta}$ (Y123), $Bi_2Sr_2Ca_2Cu_3O_{10+\delta}$ (Bi2223), $(Pr,Nd)_{2-x}Ce_xCuO_{4+\delta}$ ((Pr, Nd)214), and $Sr_{1-x}La_xCuO_2$ (SrLaCuO)) and the oxygen-based 1111 system (F-doped LaFeAsO and SmFeAsO ((La,Sm)FeAsO-F)) are taken from refs. [38,39]. The data of K-doped $BaFe_2As_2$ (Ba122-K), MgB_2, and $NbSe_2$ are taken from refs. [33,40,41], respectively. The result of $CaFe_{0.88}Co_{0.12}AsF$ (CaFeAsF-Co) is from the present work

plane. In this case, $\tilde{\rho}_s^{ab}$ of the ith FS can be given by[36]

$$\tilde{\rho}_i^{ab}(T) = 1 + 2\int_{\Delta_i}^{\infty} dE \frac{\partial f(E)}{\partial E} \frac{E}{\sqrt{E^2-\Delta_i^2}}, \quad (2)$$

where $f(E)$ is the Fermi function and Δ_i is the value of the energy gap in the ith FS. The temperature dependence of Δ_i was calculated based on the simple weak-coupling BCS model. Evidently, the kink feature around $T_c/2$ in Fig. 3 could not be described by an isotropic single gap model. In order to simplify the discussion, here we adopt a two-gap model and the total normalized superfluid density can be expressed as

$$\tilde{\rho}_s^{ab}(T) = w_1\tilde{\rho}_1^{ab}(T) + w_2\tilde{\rho}_2^{ab}(T), \quad (3)$$

$$w_i \propto \oint dS_{F,i} \frac{\vec{v}_F^{ab}\cdot\vec{v}_F^{ab}}{v_F^{ab}}. \quad (4)$$

Here, $dS_{F,i}$ indicates an integral over the ith FS and v_F^{ab} is the component of Fermi velocity within the ab plane.[36] By tuning the values of Δ_i and w_i, a simulating curve well describing the experimental data was obtained, as shown by the blue solid curve in Fig. 3. This consistency between our data and the fitting curve suggests that the two-gap model has grasped key features of this system. The two dashed lines reveal the contributions from the two components with $\Delta_1 = 0.86$ meV, $w_1 = 0.74$, and $\Delta_2 = 4.48$ meV, $w_2 = 0.26$.

DISCUSSION

Investigating the weighting factor w_i allows us to seek out the locations of the different superfluid components on the FSs. For the roughly isotropic FSs and isotropic v_F^{ab}, w_i is only determined by the v_F^{ab} value and the size of the ith FS (see Eq. (4)). Although the detailed correlation is diverse, both the nesting and local scenarios imply that the gap value is determined by the shape and size of the FSs,[13,17–19] which can be derived from the calculated electronic structures. As shown in Fig. 4a, roughly the five FSs can be divided into two groups from the viewpoint of FS shape and size: the small α FS and the large ones ($\beta/\gamma/\delta/\eta$) with similar sizes. Thus we only need to simply discuss and compare the two groups. By checking the energy dispersion of the calculated band structure, we estimated that the in-plane v_F^{ab} on the α FS is 1.25–2 times of that on the large ones ($\beta/\gamma/\delta/\eta$). As for the FS size, however, α FS is only 1/4 of the latter. Moreover, the number of the larger FSs is four, while only one small FS is present. Considering the above factors, the weighting factor of the α FS should be clearly smaller than that of the others. Consequently, we ascribe the w_2 and Δ_2 to superfluid on the α FS.

The α FS, which has a rather bad nesting condition with other FSs, carried the superfluid with a larger gap. Evidently, this is inconsistent with the nesting scenario for the pairing mechanism. Based on the local antiferromagnetic exchange pairing, which considered the local antiferromagnetic exchange of nearest neighboring and next nearest neighbor irons, a simple gap function was proposed:[13]

$$|\Delta(k)| = \Delta_0|\cos k_x \cos k_y|. \quad (5)$$

The distribution of the gap value $|\Delta(k)|$ in the Brillouin zone is displayed in Fig. 4a by the colormap. Obviously the gap value is larger on the smaller α FS, compared with other FSs, which is qualitatively consistent with our experimental result. So the local scenario is favored for the pairing mechanism of the present system. Since both the two-gap model and the gap function (Eq. (5)) are simplified with considerable approximations, we could not carry out a precise and quantitative comparison between the experimental results and the theoretical simulations at the present stage.

Previously we estimated the value of the in-plane penetration depth $\lambda_{ab}^{ab}(0)$ at 0 K based on the magnetic torque data.[26] At that time, only the $\lambda_{ab}^{ab}(T)$ data in the $T_c/2 \le T \le T_c$ range were obtained and the kink was not recognized. With the more comprehensive information now, we can update $\lambda_{ab}(0)$ to a more precise value, 260 nm. Based on this value, we checked the Uemura plot[37] which is a scaling behavior between T_c and λ_{ab}^{-2} for the SC systems with a low superfluid density. From Eq. (1), we have known that λ_{ab}^{-2} is proportional to the density of superfluid. As shown in Fig. 4b, the data of high-T_c cuprates,[38] FeSCs,[33,38,39] MgB_2,[40] and $NbSe_2$[41] are displayed together. It is clear that the hole-doped cuprates and the 1111 system of FeSCs reveal a low-superfluid-density feature and follow the linear relation of the Uemura plot. The data point represented by the yellow asterisk is from the present work and rather consistent with the results of other oxygen-based 1111 systems.

To summarize, we conduct magnetization measurements on $CaFe_{0.88}Co_{0.12}AsF$ single crystals, and the out-of-plane lower critical field H_{c1}^c is extracted. It is found that the temperature

dependent H_{c1}^{c} exhibits a pronounced kink around $T_c/2$, which can be described by a two-gap model. Importantly, the lower superfluid density with a rather large gap is attributed to the small α FS, from which the local antiferromagnetic exchange pairing mechanism is identified to be a better candidate for understanding the unconventional superconductivity of FeSCs. Moreover, our data follow the Uemura plot quite well, indicating a low-superfluid-density feature resembling the hole-doped high-T_c cuprates.

METHODS

Sample preparation

High-quality $CaFe_{0.88}Co_{0.12}AsF$ single crystals were grown using CaAs as the self-flux.[22,23] The detailed growth conditions and the characterizations of the samples can be seen in our previous reports.[23]

Magnetization measurements

The magnetization measurements were carried out on the magnetic property measurement system (Quantum Design, MPMS 3). The magnetic fields were applied along the c axis of the single crystal in all the measurements.

Band structure calculations

The first-principles calculations presented in this work were performed using the all-electron full potential linear augmented plane wave plus local orbitals method[42] as implemented in the WIEN2K code.[43] The exchange-correlation potential was calculated using the generalized gradient approximation as proposed by Perdew, Burke, and Ernzerhof.[44] The calculations for the parent compound were performed using the experimental crystal structure.[22] The band structures for the Co-doped compound were obtained by a slight shift from the results of the parent samples based on a rigid model.

DATA AVAILABILITY

All relevant data are available from the corresponding author.

ACKNOWLEDGEMENTS

This work is supported by the Youth Innovation Promotion Association of the Chinese Academy of Sciences (No. 2015187), Natural Science Foundation of China (Nos. 11204338 and 11404359), and the "Strategic Priority Research Program (B)" of the Chinese Academy of Sciences (No. XDB04040300).

AUTHOR CONTRIBUTIONS

G.M. designed the experiments. T.W. and Y.M. synthesized the samples and performed the measurements. W.L. performed the band structure calculations. G.M. analyzed the data and wrote the paper. T.W., Y.M., W.L., J.C., L.W., J.F., H.X., Z.L., T.H., X. L., and G.M. discussed the results.

ADDITIONAL INFORMATION

Competing interests: The authors declare no competing interests.

Publisher's note: Springer Nature remains neutral with regard to jurisdictional claims in published maps and institutional affiliations.

REFERENCES

1. Kamihara, Y., Watanabe, T., Hirano, M. & Hosono, H. Iron-based layered superconductor $La[O_{1-x}F_x]FeAs$ ($x = 0.05$–0.12) with $T_c = 26$ K. *J. Am. Chem. Soc.* **130**, 3296–3297 (2008).
2. Hirschfeld, P. J., Korshunov, M. M. & Mazin, I. I. Gap symmetry and structure of Fe-based superconductors. *Rep. Prog. Phys.* **74**, 124508 (2011).
3. Mazin, I. I., Singh, D. J., Johannes, M. D. & Du, M. H. Unconventional superconductivity with a sign reversal in the order parameter of $LaFeAsO_{1-x}F_x$. *Phys. Rev. Lett.* **101**, 057003 (2008).
4. Raghu, S., Qi, X.-L., Liu, C.-X., Scalapino, D. J. & Zhang, S.-C. Minimal two-band model of the superconducting iron oxypnictides. *Phys. Rev. B* **77**, 220503 (2008).
5. Ma, F., Lu, Z.-Y. & Xiang, T. Arsenic-bridged antiferromagnetic superexchange interactions in LaFeAsO. *Phys. Rev. B* **78**, 224517 (2008).
6. Yildirim, T. Origin of the 150-K anomaly in LaFeAsO: competing antiferromagnetic interactions, frustration, and a structural phase transition. *Phys. Rev. Lett.* **101**, 057010 (2008).
7. Si, Q. & Abrahams, E. Strong correlations and magnetic frustration in the high T_c iron pnictides. *Phys. Rev. Lett.* **101**, 076401 (2008).
8. Borisenko, S. V. et al. Superconductivity without nesting in LiFeAs. *Phys. Rev. Lett.* **105**, 067002 (2010).
9. Guo, J. et al. Superconductivity in the iron selenide $K_xFe_2Se_2$ ($0 \le x \le 1.0$). *Phys. Rev. B* **82**, 180520 (2010).
10. Zhang, Y. et al. Nodeless superconducting gap in $A_xFe_2Se_2$ (A = K,Cs) revealed by angle-resolved photoemission spectroscopy. *Nat. Mater.* **10**, 273–277 (2011).
11. Wang, X.-P. et al. Strong nodeless pairing on separate electron Fermi surface sheets in (Tl, K)$Fe_{1.78}Se_2$ probed by ARPES. *Europhys. Lett.* **93**, 57001 (2011).
12. Mou, D. et al. Distinct Fermi surface topology and nodeless superconducting gap in a $(Tl_{0.58}Rb_{0.42})Fe_{1.72}Se_2$ superconductor. *Phys. Rev. Lett.* **106**, 107001 (2011).
13. Seo, K., Bernevig, B. A. & Hu, J. Pairing symmetry in a two-orbital exchange coupling model of oxypnictides. *Phys. Rev. Lett.* **101**, 206404 (2008).
14. Xu, Y.-M. et al. Observation of a ubiquitous three-dimensional superconducting gap function in optimally doped $Ba_{0.6}K_{0.4}Fe_2As_2$. *Nat. Phys.* **7**, 198–202 (2011).
15. Miao, H. et al. Isotropic superconducting gaps with enhanced pairing on electron Fermi surfaces in $FeTe_{0.55}Se_{0.45}$. *Phys. Rev. B* **85**, 094506 (2012).
16. Hu, J. P. & Ding, H. Local antiferromagnetic exchange and collaborative Fermi surface as key ingredients of high temperature superconductors. *Sci. Rep.* **2**, 381 (2012).
17. Mazin, I. & Schmalian, J. Pairing symmetry and pairing state in ferropnictides: theoretical overview. *Physica C* **469**, 614–627 (2009).
18. Graser, S., Maier, T. A., Hirschfeld, P. J. & Scalapino, D. J. Near-degeneracy of several pairing channels in multiorbital models for the Fe pnictides. *New J. Phys.* **11**, 025016 (2009).
19. Ding, H. et al. Observation of Fermi-surface-dependent nodeless superconducting gaps in $Ba_{0.6}K_{0.4}Fe_2As_2$. *Europhys. Lett.* **83**, 47001 (2008).
20. Zhao, L. et al. Multiple nodeless superconducting gaps in $(Ba_{0.6}K_{0.4})Fe_2As_2$ superconductor from angle-resolved photoemission spectroscopy. *Chin. Phys. Lett.* **25**, 4402–4405 (2008).
21. Nakayama, K. et al. Superconducting gap symmetry of $Ba_{0.6}K_{0.4}Fe_2As_2$ studied by angle-resolved photoemission spectroscopy. *Europhys. Lett.* **85**, 67002 (2009).
22. Ma, Y. H. et al. Growth and characterization of millimeter-sized single crystals of CaFeAsF. *Supercond. Sci. Technol.* **28**, 085008 (2015).
23. Ma, Y. H. et al. Growth and characterization of $CaFe_{1-x}Co_xAsF$ single crystals by CaAs flux method. *J. Cryst. Growth* **451**, 161–164 (2016).
24. Terashima, T. et al. Fermi surface with dirac fermions in CaFeAsF determined via quantum oscillation measurements. *Phys. Rev. X* **8**, 011014 (2018).
25. Xiao, H. et al. Superconducting fluctuation effect in $CaFe_{0.88}Co_{0.12}AsF$. *J. Phys. Condens. Matter* **28**, 455701 (2016).
26. Xiao, H. et al. Angular dependent torque measurements on $CaFe_{0.88}Co_{0.12}AsF$. *J. Phys. Condens. Matter* **28**, 325701 (2016).
27. Ma, Y. H. et al. Strong anisotropy effect in iron-based superconductor $CaFe_{0.882}Co_{0.118}AsF$. *Supercond. Sci. Technol.* **30**, 074003 (2017).
28. Xu, B. et al. Optical study of dirac fermions and related phonon anomalies in the antiferromagnetic compound CaFeAsF. *Phys. Rev. B* **97**, 195110 (2018).
29. Ma, Y. H. et al. Magnetic-field-induced metal–insulator quantum phase transition in CaFeAsF near the quantum limit. *Sci. China Phys. Mech. Astron.* **61**, 127408 (2018).
30. Gao, B., Ma, Y., Mu, G. & Xiao, H. Pressure-induced superconductivity in parent CaFeAsF single crystals. *Phys. Rev. B* **97**, 174505 (2018).
31. Mu, G. & Ma, Y. Single crystal growth and physical property study of 1111-type Fe-based superconducting system CaFeAsF. *Acta Phys. Sin.* **67**, 177401 (2018).
32. Nekrasov, I. A., Pchelkina, Z. V. & Sadovskii, M. V. Electronic structure of new AFFeAs prototype of iron arsenide superconductors. *JETP Lett.* **88**, 679–682 (2008).
33. Ren, C. et al. Evidence for two energy gaps in superconducting $Ba_{0.6}K_{0.4}Fe_2As_2$ single crystals and the breakdown of the uemura plot. *Phys. Rev. Lett.* **101**, 257006 (2008).
34. Wang, Z. C. et al. Giant anisotropy in superconducting single crystals of $CsCa_2Fe_4As_4F_2$. *Phys. Rev. B* **99**, 144501 (2019).
35. Abdel-Hafiez, M. et al. Temperature dependence of lower critical field $H_{c1}(T)$ shows nodeless superconductivity in FeSe. *Phys. Rev. B* **88**, 174512 (2013).
36. Carrington, A. & Manzano, F. Magnetic penetration depth of MgB_2. *Physica C* **385**, 205–214 (2003).

37. Uemura, Y. J. et al. Basic similarities among cuprate, bismuthate, organic, chevrel-phase, and heavy-fermion superconductors shown by penetration-depth measurements. *Phys. Rev. Lett.* **66**, 2665–2668 (1991).
38. Luetkens, H. et al. Field and temperature dependence of the superfluid density in $LaFeAsO_{1-x}F_x$ superconductors: a muon spin relaxation study. *Phys. Rev. Lett.* **101**, 097009 (2008).
39. Drew, A. J. et al. Coexistence of magnetic fluctuations and superconductivity in the pnictide high temperature superconductor $SmFeAsO_{1-x}F_x$ measured by muon spin rotation. *Phys. Rev. Lett.* **101**, 097010 (2008).
40. Manzano, F. et al. Exponential temperature dependence of the penetration depth in single crystal MgB_2. *Phys. Rev. Lett.* **88**, 047002 (2002).
41. Fletcher, J. D. et al. Penetration depth study of superconducting gap structure of 2H-$NbSe_2$. *Phys. Rev. Lett.* **98**, 057003 (2007).
42. Singh, D. J. & Nordstrom, L. *Planewaves, Pseudopotentials, and the LAPW Method*. (Springer-Verlag, Berlin, 2006).
43. Blaha, P., Schwarz, K., Madsen, G., Kvasnicka, D. & Luitz, J. *An Augmented Plane-Wave + Local Orbitals Program for Calculating Crystal Properties*. (Technical Universität Wien, Austria, 2001).
44. Perdew, J. P., Burke, K. & Ernzerhof, M. Generalized gradient approximation made simple. *Phys. Rev. Lett.* **77**, 3865–3868 (1996).